Biogeosciences Discuss., 11, 107–149, 2014
www.biogeosciences-discuss.net/11/107/2014/
doi:10.5194/bgd-11-107-2014
© Author(s) 2014. CC Attribution 3.0 License.

Biogeosciences Discussions
Open Access

This discussion paper is/has been under review for the journal Biogeosciences (BG). Please refer to the corresponding final paper in BG if available.

Towards multi-tracer data-assimilation: biomass burning and carbon isotope exchange in SiBCASA

I. R. van der Velde[1], J. B. Miller[2,3], K. Schaefer[4], G. R. van der Werf[5], M. C. Krol[1], and W. Peters[1,6]

[1]Meteorology and Air Quality, Wageningen University, Wageningen, the Netherlands
[2]NOAA Earth System Research Laboratory, Boulder, Colorado, USA
[3]CIRES, University of Colorado, Boulder, Colorado, USA
[4]National Snow and Ice Data Center, University of Colorado, Boulder, Colorado, USA
[5]Faculty of Earth and Life Sciences, VU University, Amsterdam, the Netherlands
[6]Centre for Isotope Research, University of Groningen, Groningen, the Netherlands

Received: 22 November 2013 – Accepted: 4 December 2013 – Published: 3 January 2014

Correspondence to: I. R. van der Velde (ivar.vandervelde@wur.nl)

Published by Copernicus Publications on behalf of the European Geosciences Union.

Abstract

We present an enhanced version of the SiBCASA photosynthetic/biogeochemical model for a future integration with a multi-tracer data-assimilation system. We extended the model with (a) biomass burning emissions from the SiBCASA carbon pools using remotely sensed burned area from Global Fire Emissions Database (GFED) version 3.1, (b) a new set of ^{13}C pools that cycle consistently through the biosphere, and (c), a modified isotopic discrimination scheme to estimate variations in ^{13}C exchange as a response to stomatal conductance. Previous studies suggest that the observed variations of atmospheric $^{13}C/^{12}C$ are driven by processes specifically in the terrestrial biosphere rather than in the oceans. Therefore, we quantify in this study the terrestrial exchange of CO_2 and $^{13}CO_2$ as a function of environmental changes in humidity and biomass burning.

Based on an assessment of observed respiration signatures we conclude that SiBCASA does well in simulating global to regional plant discrimination. The global mean discrimination value is 15.2 ‰, and ranges between 4 and 20 ‰ depending on the regional plant phenology. The biomass burning emissions (annually and seasonally) compare favorably to other published values. However, the observed short-term changes in discrimination and the respiration ^{13}C signature are more difficult to capture. We see a too weak drought response in SiBCASA and too slow return of anomalies in respiration. We demonstrate possible ways to improve this, and discuss the implications for our current capacity to interpret atmospheric ^{13}C observations.

1 Introduction

A key challenge in current carbon cycle research is the estimation of the terrestrial and ocean carbon fluxes and understanding their variability. The accumulation of atmospheric CO_2 represents the sum of all sources and sinks and is currently widely used to close the carbon budget. For example, in the year 2010 9.1 ± 0.5 Pg C (= 10^{15} g) was

BGD
11, 107–149, 2014

CC BY

emitted to the atmosphere as a result of fossil fuel emissions and cement manufacture. Land use change added another 0.9 ± 0.7 Pg C to the atmosphere. The sum of these emissions together put an additional burden of CO_2 in the atmosphere (5.0 ± 0.2 Pg C), with the remainder taken up by the terrestrial biosphere and oceans (Peters et al., 2011). How much ends up in the oceans and land remains hard to quantify.

Fortunately, as more and more isotope tracer observations become available we have now the opportunity to use ^{13}C to tell us more about the different exchange processes of carbon absorbed by terrestrial biosphere and oceans. For example, measurements of the $^{13}C/^{12}C$ ratio in atmospheric CO_2 (designated as δ_a) have been used as an additional tracer alongside mole fractions of CO_2 (e.g. Keeling and Revelle, 1985; Siegenthaler and Oeschger, 1987; Keeling et al., 1989; Nakazawa et al., 1993; Tans et al., 1993; Ciais et al., 1995; Rayner et al., 2008; Alden et al., 2010). Plants assimilate the heavier $^{13}CO_2$ molecules less efficiently than $^{12}CO_2$ (by about 2 %), whereas net ocean exchange does not significantly discriminate against the heavier isotope (just 0.2 %). The most dominant photosynthetic pathways in the terrestrial biosphere (C_3) also discriminates significantly more than the less common C_4 pathway (about 1.4 %). Therefore, patterns in atmospheric CO_2 and δ_a together can potentially provide more insights on the carbon fluxes than with only CO_2 as tracer.

The heterogeneous structure of the terrestrial biosphere and its response to weather and climate make CO_2 and $^{13}CO_2$ exchange variable in space and time. The extent to which plants discriminate against $^{13}CO_2$ is strongly dependent on environmental conditions acting on the photosynthesis. A combination of atmospheric humidity, precipitation, and soil moisture are factors that determine the stomatally induced variations in isotopic discrimination (Farquhar et al., 1989; Wingate et al., 2010). In addition, the global distribution of C_3 and C_4 plants affect the global mean discrimination strongly (Still et al., 2003). The respiration of older carbon back to the atmosphere that is heavier in ^{13}C than newly assimilated carbon acts as an additional flux of $^{13}CO_2$ molecules towards the atmosphere (disequilibrium flux). This effect stems from a constant dilution of δ_a by isotopically depleted CO_2 from fossil fuel combustion (also known as the

BGD
11, 107–149, 2014

Suess effect; Suess, 1955; Keeling, 1979). Errors in the representation of disequilibrium fluxes can lead to errors in the estimated land/ocean mean flux partitioning, as well as in the estimated variability of each sink. For example, an underestimation in the calculated isotopic signature of the carbon pools, or their turnover could cause an underestimate of the disequilibrium flux, requiring a change in the estimated partitioning of the net biosphere flux and ocean flux. Much effort therefore goes into improving the realism of ocean and biosphere carbon exchange and its impact on the isotopic ratio.

A similar argument can be made for flux variability. Alden et al. (2010) and van der Velde et al. (2013) showed that observed variability in $^{13}CO_2$ is difficult to reproduce when ocean variability is assumed low. To close the atmospheric ^{13}C budget the variability in the biosphere must be larger than currently accounted for in SiBCASA (van der Velde et al., 2013). Therefore, the current lack of understanding of the atmospheric budget is an important justification to explore isotope exchange with the atmosphere and the terrestrial biosphere in more detail.

In the past, significant attention has been paid to realistically simulate the seasonal and spatial variations of C_3 and C_4 plant discrimination, by simulating the coupling between carbon assimilation and leaf CO_2 concentration on monthly time intervals (e.g. Lloyd and Farquhar, 1994; Fung et al., 1997). In recent studies more detailed process descriptions have been used to estimate plant discrimination (e.g. Kaplan et al., 2002; Suits et al., 2005), but these models could not simulate the isotopic disequilibrium because they lacked descriptions of terrestrial carbon pools. Scholze et al. (2003 and 2008) developed in the Lund-Potsdam-Jena dynamic vegetational model (LPJ) a full terrestrial cycling framework of CO_2 and $^{13}CO_2$. This model included the isotopic fractionation model of Kaplan et al. (2002) and above and below ground biogeochemical pools to store the total carbon and ^{13}C consistently.

Carbon surface flux estimates by the current data-assimilation methods are consistent with the observed history of atmospheric CO_2 (e.g. Gurney et al., 2002; Peters et al., 2007). However, their capacity is often limited by the number of CO_2 observations and the realism of the bottom-up carbon exchange estimates. These methods

BGD
11, 107–149, 2014

often misallocate the CO_2 uptake of the land biosphere with the oceans, and are not well suited to study processes underlying the exchange. To provide a better constraint on the carbon cycle we are currently developing a multi-tracer carbon cycle data-assimilation framework that includes not only observations and bottom-up estimates of CO_2, but also observations of δ_a and the exchange of $^{13}CO_2$ at the earth surface. Such framework requires above all a realistic $^{13}CO_2$ flux estimate from the biosphere which is difficult to quantify but is found to be an important term in atmospheric δ_a budget (van der Velde et al., 2013). Over land variations in δ_a reflect differences in the strength of plant discrimination but also varies as a function of moisture conditions and can inform thus on drought stress. Another important requisite over land is biomass burning as they shorten the turnover time of carbon in the terrestrial biosphere, and therefore influence the disequilibrium flux. In addition, it is the largest source of CO_2 in the tropics, and because of its intermitted nature it contributes to the interannual variability of CO_2 and $^{13}CO_2$ in the atmosphere. An additional advantage of the integrated biomass burning is the possibility to simulate CO emissions, a tracer with much potential to constrain the tropical fire emissions (van der Werf et al., 2008).

Towards such integrated data-assimilation framework we present here two novel additions to the SiBCASA biosphere/biogeochemical model: firstly, a realistic yet simple representation of fire emissions that are consistent with the predicted amount of standing biomass, and secondly, a framework of ^{13}C exchange. We investigate how the new model performs compared to similar models and observations, and where there is need for improvements. It builds upon the work of Schaefer et al. (2008), who developed the original SiBCASA terrestrial biosphere model that combines the prediction of photosynthesis with the allocation of biomass. We included an isotopic discrimination parameterization scheme slightly modified from that of Suits et al. (2005) to estimate on a high time and spatial resolution isotopic composition within the plant. Our aim is three-fold: (1) to evaluate SiBCASA biomass burning against state of the art estimates from CASA-GFED3 (van der Werf et al., 2010). (2) To compare simulated discrimination and disequilibrium fields with the published literature. And (3), to simulate

BGD
11, 107–149, 2014

CC BY

the short-term plant discrimination and the response to environmental conditions, and compare those with observations.

2 Methodology

2.1 SiBCASA model

The SiBCASA model (Schaefer et al., 2008) combines two biogeochemical process models in a single framework. The biophysical part of the model is based on the Simple Biosphere model, version 3 (SiB, Sellers et al., 1996), with the carbon biogeochemistry from the Carnegie-Ames-Stanford Approach (CASA, Potter et al., 1993) model. The joint model framework calculates at 10 min time steps and on a spatial resolution of $1^\circ \times 1^\circ$ the exchange of carbon, energy and water. In the canopy air space, the CO_2 concentration, temperature and humidity are calculated as prognostic variables (Vidale and Stockli, 2005). Effects of rainfall, snow cover, and aerodynamic turbulence are included in the computation of the latent and sensible heat fluxes (Sellers et al., 1996).

For plant photosynthesis, SiBCASA uses the Ball-Berry stomatal conductance model as modified by Collatz et al. (1991) coupled to a modified version of the Farquhar et al. (1980) C_3 enzyme kinetic model and the Collatz et al. (1992) C_4 photosynthesis model. Leaf photosynthesis is scaled to the canopy level using absorbed fraction of Photosynthetically Active Radiation (fPAR) derived from remotely sensed AVHRR Normalized Difference Vegetation Index (NDVI, Sellers et al., 1994, 1996a, b).

The photosynthetic carbon flux is calculated for two physiological plant types (currently C_3 and C_4). The global $1^\circ \times 1^\circ$ map with the fraction of C_4 plants is provided by Still et al. (2003). For the grid cells that contain a fraction of both C_3 and C_4 plant types, the uptake and respiration fluxes of each of the plant types are computed separately, and are subsequently combined depending on their fractional coverage to get grid cell average fluxes.

BGD
11, 107–149, 2014

As displayed in Fig. 1a, the total carbon ($^{13}C + ^{12}C$) that is photosynthesized is allocated to a series of different live carbon pools (leave, root, wood), surface litter pools (coarse woody debris, metabolic, structural and microbial) and layered soil pools (metabolic, structural, microbial, slow, and armored). The amount of carbon in each of the 13 biogeochemical pools is solved prognostically as a first order linear differential equation depending on gains from other pools, losses to other pools and respiration losses due to (heterotrophic) microbial decay and (autotrophic) plant growth (Schaefer et al., 2008). The leaf pool is somewhat special because its carbon stocks are computed semi-prognostically. This means that the leaf pool is prognostic, but the photosynthesis calculations are constrained by remotely sensed leaf area.

$^{13}CO_2$ fluxes are computed in the isotopic discrimination model that we implemented in SiBCASA (see Sect. 2.2). We keep the ^{13}C stocks separated from the total carbon stocks by defining 13 additional biogeochemical pools for ^{13}C alone. Similar to total carbon, ^{13}C is transferred from one pool to another as shown in Fig. 1a. For now, no discrimination effects are considered for transfers of carbon between pools and during respiration. The average turnover times, and the scaling factors for temperature, freezing and moisture were taken from the original SiBCASA scheme.

2.2 Isotopic discrimination

Inherited from the SiB2.5 model is the CFRAX (carbon fractionation) scheme to calculate the $^{13}C/^{12}C$ isotopic ratios in the terrestrial exchange fluxes of CO_2 (Suits et al., 2005). These ratios are the result of several discrimination effects during the photosynthetic uptake of CO_2, where plants favor taking up the more abundant $^{12}CO_2$ molecules rather than the heavier $^{13}CO_2$ molecules. From atmosphere to plant interior SiBCASA identifies three transport stages, where at each stage the CO_2 concentration is slightly altered due to a resistance. Similarly, these stages are also associated with discrimination against $^{13}CO_2$. These discrimination effects are expressed as Δ in per mille, which are indicative how much the isotopic ratio from one location to the next will change.

BGD
11, 107–149, 2014

See the Appendix for a more detailed explanation on how to interpret the notation of isotopes and discrimination in this publication.

The total discrimination for C_3 plants (Δ_{C3}) is given by a weighted-sum of all the transfer stages that are associated with photosynthesis (Farquhar, 1983):

$$\Delta_{C3} = \Delta_b \left(\frac{C_a - C_s}{C_a}\right) + \Delta_s \left(\frac{C_s - C_i}{C_a}\right) + \left(\Delta_{diss} + \Delta_{aq}\right) \left(\frac{C_i - C_c}{C_a}\right) + \Delta_f \left(\frac{C_c}{C_a}\right), \quad (1)$$

where $C_{a,\,s,\,i,\,c}$ represent the CO_2 concentrations in canopy air space, leaf boundary layer, stomatal cavity, and the chloroplasts. The separate isotope effects are constant and determined from theoretical calculations and laboratory experiments (Craig, 1953; Farquhar, 1983; Mook et al., 1974; O'Leary, 1984). Two of them are related to molecular diffusion from canopy air space to leaf boundary layer (Δ_b = 2.9 ‰) and molecular diffusion through the leaf stomata (Δ_s = 4.4 ‰). Subsequently, smaller isotope effects occur during the dissolution of CO_2 in mesophyll and transport to the chloroplast (Δ_{diss} = 1.1 and Δ_{aq} = 0.7 ‰). The largest isotope effect is associated with the fixation of CO_2 by the enzyme Rubisco and a small fraction by phosphoenyl pyruvate carboxylase (PEPC) enzyme in the chloroplast (Δ_f = 28.2 ‰). A schematic representation of Eq. (1) in relation to the flow of carbon is given in Fig. 3 in the publication of Suits et al. (2005).

Because the separate isotope effects are assumed constant, variability in Δ_{C3} depends on the concentration gradient between the canopy air space and the leaf interior, which depends on the opening and closing of leaf stomata, which we represent as stomatal conductance. For instance, water deficiency would generally close the leaf stomata and decrease the stomatal conductance, resulting in a drop of the plant interior CO_2 concentrations (C_i and C_c). Consequently, a large CO_2 gradient will exist between the ambient atmosphere and interior plant. The discrimination term associated with CO_2 fixation by Rubisco (last term in Eq. 1) will disappear, as the ratio C_c/C_a approaches zero. However, at the same time, more weight will be assigned to discrimination associated with molecular diffusion through the leaf stomata. When there is no

BGD
11, 107–149, 2014

CC BY

water stress, the opposite will happen. Stomata remain open, and therefore, a small CO_2 gradient will exist, which keeps the C_c/C_a ratio large, and thus more weight is assigned to the Rubisco fixation stage.

For C_4 plants, we assume that all of the available carbon is fixed by PEPC. Therefore, similar to Suits et al. (2005), we only assume an isotopic effect associated with molecular diffusion at the leaf stomata, i.e. $\Delta_{C4} = 4.4\,‰$. Brüggemann et al. (2011) discuss several other possible fractionation steps associated with the transport of organic matter between different plant tissues, however such processes are not included in our model since the availability of such data remains scarce. For both C_3 and C_4 plants we do not take into account isotope effects that are associated with respiration as their contributions are poorly understood (Scholze et al., 2008). The isotopic discrimination value (denoted as Δ, which can either refer to Δ_{C3} or Δ_{C4}), is used to compute the ^{13}C and ^{12}C flux ratios of total carbon assimilation (F_a), canopy respiration ($F_{respcan}$) and net assimilation ($F_n = F_a - F_{respcan}$).

The $^{13}C/^{12}C$ ratio in the current net assimilated plant material (R_n) is determined using the relationship between discrimination Δ and the isotopic ratio of the atmosphere (R_{atm}):

$$R_n = \frac{R_{atm}}{\left(\frac{\Delta}{1000} + 1\right)}, \tag{2}$$

and is discussed in more detail in the Appendix. Subsequently, the ^{13}C and ^{12}C net assimilation rates are calculated by

$$^{13}F_n = \frac{R_n \cdot F_n}{1 + R_n}, \tag{3}$$

$$^{12}F_n = \frac{F_n}{1 + R_n}. \tag{4}$$

The latter two fluxes are calculated separately for physiological plant types C_3 and C_4 and, in combination with the prescribed fraction of C3 plants (β), a gridcell averaged

BGD
11, 107–149, 2014

flux is calculated:

$$^{13}F_{\mathrm{n}} = {}^{13}F_{\mathrm{n,\,c3}} \cdot \beta + {}^{13}F_{\mathrm{n,\,c4}} \cdot (1-\beta), \tag{5}$$

$$^{12}F_{\mathrm{n}} = {}^{12}F_{\mathrm{n,\,c3}} \cdot \beta + {}^{12}F_{\mathrm{n,\,c4}} \cdot (1-\beta). \tag{6}$$

Compared to original version of CFRAX we have improved the treatment of respiration. Respiration was given the isotope ratio of the long-term integrated net assimilation. In our version the carbon source for canopy respiration changes from day to night. During the day, when there is net assimilation, we assume the most recently assimilated starch is used for the canopy respiration. Therefore, we make the assumption that the $^{13}C/^{12}C$ ratio of canopy respiration equals the isotopic ratio in the assimilation rate ($R_{\mathrm{respcan}} = R_n$).

During the transition from day to night, when photosynthesis ceases, the carbon source for canopy respiration switches to whole-plant starch reserves (i.e., the storage pool). In reality, as photosynthesis declines, we expect that such a transition would go smoother, where there is a more gradual switching between the two carbon sources. Such a gradual transition is not yet realized. Subsequently, the net assimilation flux feeds the storage pool with carbon.

Because output is written at monthly or daily time intervals, the total discrimination factor Δ must be an assimilation-weighted average since discrimination at night when photosynthesis is zero makes no sense. Therefore, over t number of timesteps, we compute for each land point:

$$\Delta_{\mathrm{month}} = \frac{\sum^{t} \Delta_t \cdot F_{\mathrm{a,\,t}}}{\sum^{t} F_{\mathrm{a,\,t}}}. \tag{7}$$

2.3 Disequilibrium flux

In the ^{13}C budget we must take into account disequilibrium flux which does not appear in the total carbon budget. This so-called disequilibrium flux exist because of

BGD
11, 107–149, 2014

CC BY

a long-term draw down of the atmospheric $^{13}C/^{12}C$ ratio due to fossil fuel emissions of isotopically light CO_2 (e.g. Francey et al., 1999). Therefore, the older carbon that is released to the atmosphere is richer in ^{13}C compared to the carbon that is currently taken up by the oceans and land. For the terrestrial biosphere, this isotopic difference is designated as the isodisequilibrium forcing coefficient (Alden et al., 2010), and can separately be defined for biological respiration $I_{ba} = \delta_{ba} - \delta_{ab}$ and for biomass burning $I_{fire} = \delta_{fire} - \delta_{ab}$ (van der Velde et al., 2013). These isotopic differences are scaled by large gross fluxes: F_{ba} for biological respiration and F_{fire} for biomass burning.

The total isotopic disequilibrium flux from the terrestrial biosphere D_{bio} is defined as

$$\begin{aligned} D_{bio} &= F_{ba}\left[\delta_{ba} - \delta_{ab}\right] + F_{fire}\left[\delta_{fire} - \delta_{ab}\right] \\ &= F_{ba} I_{ba} + F_{fire} I_{fire}. \end{aligned} \tag{8}$$

where the fluxes F_{ba} and F_{fire} are given in $\mu mole\, m^{-2}\, s^{-1}$ for each grid cell. The monthly isotopic signatures associated with respiration (δ_{ba}), biomass burning (δ_{fire}) and uptake (δ_{ab}) are determined with the use of Eq. (A3), i.e.,

$$\delta_{ba} = 1000 \times \left(\frac{^{13}F_{ba}/^{12}F_{ba}}{R_{std}} - 1 \right) \tag{9}$$

$$\delta_{fire} = 1000 \times \left(\frac{^{13}F_{fire}/^{12}F_{fire}}{R_{std}} - 1 \right) \tag{10}$$

$$\delta_{ab} = 1000 \times \left(\frac{^{13}F_{a}/^{12}F_{a}}{R_{std}} - 1 \right) \tag{11}$$

2.4 Biomass fire scheme

We introduce fire combustion of total carbon and ^{13}C in SiBCASA, which is largely based on the work of van der Werf et al. (2003, 2010). Our calculated fire emissions are

BGD
11, 107–149, 2014

driven by multiple remotely sensed burned area products combined in the Global Fire Emissions Database (GFED) version 3.1 (Giglio et al., 2010). The burned area is given in hectares per month and spans the time period from July 1996 through the end of 2011. Most of the burned area is produced using Moderate Resolution Imaging Spectroradiometer (MODIS) surface reflectance imagery. The data set is extended prior to MODIS with fire observations from the Tropical Rainfall Measuring Mission (TRMM) Visible and Infrared Scanner (VIRS) and Along-Track Scanning Radiometer (ATSR). To make GFED3.1 burned area serve as input for our model, its original $0.5^\circ \times 0.5^\circ$ grid is aggregated to a total of 14 538 $1^\circ \times 1^\circ$ SiBCASA landpoints. Furthermore, the burned area is transformed to a scaling factor A by dividing the burned area (BA) with the area (GA) of each grid cell and the number of seconds per month (S):

$$A = \frac{\mathrm{BA}}{\mathrm{GA} \cdot S}. \tag{12}$$

The burned area factor A [s^{-1}], together with the tree mortality rates M (rate that relates to the density of trees in a biome), carbon stocks C and pool-dependent combustion completeness factors E (the fraction of biomass available for combustion for each pool p) determine the combustion flux of total carbon and ^{13}C:

$$F_{\mathrm{fire}} = A \cdot M \sum^{p} C_p \cdot E_p, \tag{13}$$

$$^{13}F_{\mathrm{fire}} = A \cdot M \sum^{p} {}^{13}C_p \cdot E_p, \tag{14}$$

where F_{fire} and $^{13}F_{\mathrm{fire}}$ represent the fire flux per grid cell per timestep [given in µmole $\mathrm{m}^{-2}\,\mathrm{s}^{-1}$] summed over the p number of above ground and fine litter pools. The numbers used for the combustion completeness and tree mortality are given in Table 1. The carbon flow chart for fires is given in Fig. 1b. We assume that only above ground biomass and fine litter on the surface are affected by fires. The part of the carbon that is not combusted is regarded as dead biomass and is subsequently transferred from

BGD
11, 107–149, 2014

CC BY

the above ground pools to the fine litter pools. The uncombusted carbon in the fine litter pools is not further transferred. Indonesian peat burning (Page et al., 2002) and organic soil carbon combustion in the boreal region are neglected for this publication.

2.5 Experimental setup

SiBCASA was run globally from 1851 through 2010. We assumed at the start of the simulation an approximate steady state (NEE ≈ 0), which is an assumption that is often made for biogeochemical models since observations of biomass are not available from that era (Schaefer et al., 2008). Actual driver data (meteorology, NDVI, burned area) was used only for the 1997–2009 period. Before 1997, we drive SiBCASA with a single random year from our available 13 yr input dataset, ensuring that meteorology, NDVI, and burned area come from the same year and are thus internally consistent. That means that any variability from long-term climate change effects, such as rise in global temperature are not included in these simulations. The monthly δ_a observational record spans the 1850–2008 period simulated and each year in SIBCASA thus has realistic atmospheric δ_a values, allowing us to simulate the disequilibrium between biosphere and atmosphere over time (note that climate imposed changes are not accounted for). The monthly record is based on ice-core measurements (Francey et al., 1999) and from 1989 onward based on atmospheric observations. For the past changes in atmospheric CO_2 concentration, we use a curve fit to observed global CO_2 concentrations from the ice core from Taylor Dome (Indermuhle et al., 1999) and the Globalview data product (Masarie and Tans, 1995).

Three different simulations are performed (Table 2): (1) the ISOVAR simulation (we use the same designation as Scholze et al., 2003 and 2008; van der Velde et al., 2013) includes the dynamic discrimination scheme, (2) the ISOFIX simulation uses fixed values for C_3 and C_4 plant discrimination (19.2 and 4.4 ‰ respectively), and (3) the ISOVAR simulation without fire fluxes (ISOVAR-NF, *No Fires*). Between ISOVAR and ISOVAR-NF, the total NEE remains almost the same because the excluded fire disturbances in ISOVAR-NF are compensated by increased respiration. All simulations

BGD
11, 107–149, 2014

include the same prescribed records of atmospheric CO_2 and δ_a, the same C_3/C_4 distribution, and the same SiBCASA climate driver files as described above.

3 Results

3.1 Biomass burning

Because our fire emissions estimates are based on burned area maps, their spatial patterns are similar but emissions vary widely per unit area burned, which confirms the findings of van der Werf et al. (2006). As displayed in Fig. 2a, most of the burned area covers Africa and North Australia, especially in regions dominated by savanna grasses. However, because of their relatively low fuel loads, the actual carbon emissions (Fig. 2b) from these regions are low per unit area burned. On one hand, Australia accounts over the period 1997–2009 14 % of the total burned area, but it only contributes 4 % of the total fire emissions. But on the other hand, Tropical Asia (defined as transcom region as in Gurney et al., 2002) accounts for just 2 % of the total burned area but emits 13 % of the total global fire emissions. This is mainly due to the high fuel loads in the form of aboveground wood biomass. Africa is by far the largest contributor, both in terms of emissions (53 %) and burned area (70 %). The total is equivalent to 2.55 million $km^2 yr^{-1}$ of area burned averaged over 1997 through 2009.

The annual mean and interannual variability (IAV) of the global fire flux for the period 1997–2009 is 1.93 ± 0.40 Pg C yr^{-1}, which is only 0.07 Pg C yr^{-1} smaller than reported by the fire scheme of CASA-GFED3 (van der Werf et al., 2010). As displayed in Fig. 3, the global trend and the significant IAV in fire emissions are consistent with CASA-GFED3. It captures much of the timing of years of strong and weak fire emissions. For instance, large emissions occurred in 1997 and 1998, followed by smaller emissions after 1998. We also see the same general regional characteristics, and seasonal and interannual variability as in CASA-GFED3. For instance, Eurasian Boreal fluxes are more than twice as large as the North American Boreal fluxes because its area

BGD
11, 107–149, 2014

is much larger. Globally, 2001 and 2009 are consistently the years with the lowest emissions (1.5 Pg C yr^{-1}). Some of the year-to-year differences in the annual fire emissions stem from the lack of specific combustion processes in SiBCASA mentioned in the methodology section: primarily peat and organic soil combustion. Specifically, we underestimate (relative to CASA) the global emissions in 1997, 2002, and 2006 by 0.1–0.3 Pg C yr^{-1}. An example is the fire emissions in Tropical Asia, where we miss the peak burning events in 1997, 2002, and 2006 due to the lack of peat burning in our framework. For the other years the emissions between CASA and SiBCASA are very consistent. In the North American boreal, Eurasian boreal and Eurasian temperate regions the emissions are about 50 % smaller than estimated by CASA due to lack of organic soil combustion. This is also visible in the zonal mean profile in Fig. 2b. Because these regions contribute only little to the total emissions it does not affect the global flux much. In Tropical and Temperate South America the fire emissions are overestimated through the whole period investigated. This is a consequence of larger fuel loads in SiBCASA in comparison to CASA, and differences between the coarse biome map and the remotely sensed burned area. These burned area fields are aggregated from 0.5° × 0.5° resolution to a coarser 1° × 1° resolution. Especially at the boundaries between biome types, e.g. tropical forests (high fuel load) and savannas (low fuel loads), chances are that part of the burned area is wrongly assigned to another biome with different simulated biomass giving skewed emissions. This is apparent close to the equator where we observe a large spike of emissions in the zonal mean profile in Fig. 2b. Other minor differences between the flux estimates presented here and those reported in van der Werf et al. (2010) stem from SiBCASA's more simplified representation of the fire parameters. For instance, we used a biome specific fixed combustion completeness factor, rather than a variable one.

3.2 Discrimination: global mean and trend

The largest spatial differences in the global annual plant discrimination (assimilation-weighted) are determined by the C_3/C_4 plant distribution (Fig. 4a). Regions with lower

BGD
11, 107–149, 2014

CC BY

values of discrimination correspond to the dominant presence of C_4 plants, such as the South American grasslands, African subtropical savannas, Northern Australia, and North American crop fields. Smaller differences in discrimination, within C_3 dominant areas, are caused by climate conditions, water availability and relative humidity. These parameters affect the stomatal conductance, and subsequently control Δ in Eq. (1) through changes in the ratios of CO_2 concentration in the ambient atmosphere and plant intercellular space.

The variability in C_3 discrimination for the period 1997–2008 is typically 0.15 ‰ (Fig. 4b). Most of the IAV can be seen over the mid and higher latitudes and can be attributed to variations in precipitation and relative humidity as identified by Suits et al. (2005). Over the tropical latitudes the annual variability is generally very small. Larger excursions are seen in mixed C_3 and C_4 grid cells in the South American and African subtropics. Because discrimination is different between C_3 and C_4 metabolic pathways, independent year-to-year deviations of C_3 and C_4 GPP in those cells will affect the mean discrimination value.

The global annual discrimination and IAV (assimilation-weighted) is 15.2 ± 0.04 ‰ (linear detrended and averaged for the period 1997–2008), and is, as shown in Table 3, comparable to similar studies (Lloyd and Farquhar, 1994: 14.8 ‰; Fung et al., 1997: 15.7 ‰; Suits et al., 2005: 15.9 ‰). We see larger differences with the studies of Kaplan et al. (2002) and Scholze et al. (2003). They reported values of 18.1 and 17.7 ‰ respectively because of accounting only 15 % and 10 % of the GPP to the less discriminating C_4 plants. In contrast, our model assigns around 30 % of the GPP to C_4 plants. These differences mainly depend on the vegetation database used. For instance, our C_3/C_4 distribution database (Still et al., 2003) includes additional C_4 coverage from crop fraction maps (Ramankutty and Foley, 1998), and data on crops from the *Food and Agriculture Organization*. A large part of the year-to-year changes in global discrimination are driven by shifts in C_3 and C_4 productivity (van der Velde et al., 2013).

BGD
11, 107–149, 2014

3.3 Disequilibrium: global mean and trend

The isodisequilibrium coefficient I_{bio} (combined weighted mean of I_{ba} and I_{fire}) is highly variable in space. Figure 5 displays the map of the global annual ISOVAR disequilibrium, averaged for the period 1997–2008. Generally, the values of I_{bio} are high in regions where the carbon turnover times are long such as forests and tundra. The largest values of 0.5 ‰ correspond to regions such as boreal forests in North America and the Eurasian. The lowest values of I_{bio} can be found in regions covered with herbaceous vegetation such as in the African savanna. Differences in residence times are the result of variations in plant types, respiration, and fire disturbances. Large disequilibria are mostly found in wood, which has the longest above ground turnover time (30–50 yr) and is typically the largest pool. There are no trees in tundra, but the soil carbon is frozen most of the year, resulting in effective turnover times as high as 1500 yr. In our study the total respiration carries the mean signature of old and new carbon. If we would base I_{bio} solely on heterotrophic respiration, as done in other studies, its value would become roughly 2 times larger. This is because δ signature of heterotrophic respiration (2 times smaller in magnitude than total respiration) represents an older biomass and is thus heavier in ^{13}C than total respiration, which includes also autotrophic respiration with a δ signature that is much closer to the current assimilation signature.

In 1988 (to compare with other studies), the global heterotrophic-weighted mean I_{bio} was estimated at 0.42 ‰. This value lies close to the ones found elsewhere for the same year and is summarized in Table 3. For example, Joos and Bruno (1998) and Francey et al. (1995) reported 0.43 ‰, and Scholze et al. (2008) reported a range between 0.42 and 0.59 ‰.

As shown in Fig. 6, from 1950 onward, the atmospheric isotopic composition depleted rapidly in ^{13}C due to intensified emissions of isotopically light CO_2 from fossil fuel combustion. As a response to this depletion, the disequilibrium increased rapidly from 0 Pg C ‰ yr^{-1} in 1950 to 30 Pg C ‰ yr^{-1} in the twenty-first century. The extra variability in δ_a after 1989 is from the increase in available flask measurements. Between 1997–

BGD
11, 107–149, 2014

CC BY

2008, the three simulations had the following mean values and interannual variability (from the linear trend): ISOVAR; 25.8 ± 1.5 Pg C ‰ yr^{-1}, ISOFIX; 24.3 ± 1.1 Pg C ‰ yr^{-1}, and ISOVAR-NF; 27.4 ± 1.4 Pg C ‰ yr^{-1}. The ISOVAR-NF experiment, without fire disturbances, resolves generally larger values for D_{bio} than the other two experiments. It confirms that biomass burning shortens the turnover times of the biogeochemical pools, which results in a smaller disequilibrium flux than if the turnover is determined only by natural processes, like e.g. decay of biomass. Variability in ISOVAR-NF and ISOFIX is slightly smaller than for ISOVAR because they lacked intermittency from year to year changes in biomass burning and discrimination, respectively.

Looking at spatial differences, tropical forest biome accounts for 40 % of the total disequilibrium flux. It is a combined effect of a large respiration flux (32 % of global respiration) and long pool turnover ($D_{tropics}$ = 10.4 Pg C ‰ yr^{-1} and $I_{tropics}$ = 0.27 ‰). Around 95 % of this disequilibrium flux originates from heterotrophic respiration. Boreal forest soils are generally older, but they account only for 11 % of the total disequilibrium flux (D_{boreal} = 2.8 Pg C ‰ yr^{-1} and I_{boreal} = 0.38 ‰) because productivity and respiration are much lower. Dry areas with a small amount of biomass such as the American grasslands, African savannas, parts of India and Australia, contribute little to the total disequilibrium flux.

3.4 C13 exchange: observations vs. model

To evaluate our model performance with respect to the biophysical processes that influence plant discrimination and respiration we make use of the comprehensive Biosphere–Atmosphere Stable Isotope Network (BASIN; Pataki et al., 2003). BASIN serves as an archive using a common framework for the collection and interpretation of isotopic signatures in CO_2 respiration (δ_r) using Keeling plot intercept data across sites in North and South America.

In general, our simulated δ_r values compare well with the mean observed δ_r values as shown in Fig. 7 for a selection of sites. The vegetation of most of the sites presented here is C_3, which results in a cluster of values with a respiration signature between −23

BGD
11, 107–149, 2014

and −28 ‰. The vegetation at the site in Kansas is predominately C_4 tallgrass prairie, which explains the low value of around −20 ‰. We capture similar signatures in our model, which confirms that there is agreement between actual plant use and the C_4 distribution map from Still et al. (2003). There are also differences between the model and measurements. For example, the simulated respiration signature in the tropical forest site is less negative than observed. And for Sisters, Oregon, we see the opposite. The simulated respiration signature is far more negative there than observed. A possible reason is that we misrepresent the carbon age in our model. It could be that carbon respired from the carbon pools in SiBCASA are older (reflect a less negative atmosphere) than actually measured or vice versa. However, it is more likely that we miss external variability in our model, specifically in monthly precipitation, relative humidity and soil moisture stress. Such environmental conditions can cause an abrupt change in the respiration signature, which signature is not simulated well in SiBCASA.

Several measurement experiments in the past have shown that C_3 plant discrimination is strongly dependent on fairly short-term changes in environmental conditions (Ehleringer and Cook, 1998; Ekblad and Hogberg, 2001; Bowling et al., 2002; Ometto et al., 2002). A combination of atmospheric humidity and soil water stress are considered important factors that determine the stomatal induced variations in isotopic discrimination. More importantly, the measurements suggest that it takes only a few days for carbon that is assimilated through photosynthesis to become available again through respiration from short turnover root pools. We compare the modeled assimilation-weighted discrimination and the respiration signatures with the correlation fits determined by Ekblad and Hogberg (2001) and Bowling et al. (2002). Ekblad and Hogberg measured soil respiration in a boreal forest in northern Sweden and Bowling et al. calculated Keeling plot intercepts at four different locations in Oregon. Suits et al. (2005) already compared SiB's assimilated isotopic signatures with these correlation fits. In their study the main purpose was to evaluate the relationship between humidity and discrimination in their parameterization. Because our framework now includes the

BGD
11, 107–149, 2014

complete exchange of ^{13}C we can now expand this analysis with the actual modeled respiration signatures (δ_r) from the different carbon pools to changes in humidity.

In general, the model captures the relationship between vapor pressure deficit (VPD) and daily discrimination in summer time (Fig. 8a) given by the approximate curve fits to the measurements. The modeled discrimination values are in between the two observed relationships, but the general pattern for both locations is more or less the same: a small VPD (high RH) promotes larger stomatal conductance, which increases discrimination. Strong curvature when VPD is low, as seen by Bowling et al., is not captured in our model at both locations. The gradient is more comparable to the measurements of Ekblad and Hogberg.

Important to note, these curve fits in Fig. 8a are an approximation because discrimination was not actually measured. Instead, these fits were derived from the respiration signature curve fits given the current atmospheric signature: $\Delta = \frac{\delta_a - \delta_r}{\delta_r/1000+1}$. The real discrimination values are likely several tenths of a per mille larger because the assimilated signatures are typically more depleted in ^{13}C.

The simulated values of the isotopic signature in total respiration (Fig. 8b) do not correspond well with the actual curve fits to measurements. Ekblad and Hogberg and Bowling et al. have demonstrated that variations in the isotopic signature of respiration are strongly correlated with changes in RH and VPD that have occurred within the previous 2 to 10 days. That means that a large fraction of respired CO_2 comes from the metabolism of recently fixed carbohydrates. Such strong correlation over such a short time span is not reproduced by our model. We do observe somewhat of a correlation between VPD and δ_r if VPD is lagged by about 2 months (not shown in Fig. 8). This is mostly the result of autotrophic respiration, which is calculated based on the storage pool. In other words, ^{13}C of autotrophic respiration reflects ^{13}C of the storage pool. In SiBCASA, the turnover time for the whole storage pool is prescribed at 7 days. However, based on measurements the assumption was made that only 10 % of the storage pool starch is in the form of sucrose is ready for conversion to biomass. The remaining 90 % is in the form of other carbohydrates that are not readily converted to

BGD
11, 107–149, 2014

biomass. Since a smaller portion of the storage pool is available for plant growth, the *effective* turnover time for the storage pool in SiBCASA is therefore around 70 days instead of 7 days. As a result, short term responses in the total isotopic respiration signal are lost.

We do simulate daily instantaneous fluctuations in δ_r resulting from canopy respiration, and these do correlate with changes in VPD since the signatures in canopy respiration are close to the isotopic ratio of recent assimilated carbon (Fig. 8c). Their contribution to the total simulated respiration is small though (10 %) and therefore have little impact.

4 Discussion and conclusions

In this study we introduce a modified version of SiBCASA, which can now produce ^{12}C and ^{13}C exchange. The modifications include realistic fire emissions based on remotely sensed burned area, and the exchange of ^{13}C isotopes between atmosphere and plants. A comprehensive set of observations and other model studies were used to assess the model performance. We now come back to our aims given in the Introduction.

(1) Global fire emissions compare well with estimates from the CASA-GFED3 study described in van der Werf et al. (2010). Between 1997–2009 we simulate an average flux of 1.93 Pg C yr^{-1}, which is 3.5 % less than reported in the CASA-GFED3 study. On both global and regional scales the trend, the seasonal, and the interannual variability in the fire emissions are consistent. The underestimation of fire emissions in Tropical Asia and Boreal regions are expected since our simplified approach does not include specific processes like peat combustion and organic soil combustion. Other smaller discrepancies between SiBCASA and CASA are the result of differences in the amount of biomass and mismatches between the biome type map and the remotely sensed burned area. For future research, we can make improvements such as peat and or-

BGD
11, 107–149, 2014

ganic soil combustion, and more specific combustion parameters, which can vary in time and location.

(2) Isotopic discrimination and disequilibrium signal in respiration are generally consistent with observations and comparable with similar studies. SiBCASA calculates a global annual discrimination of 15.2 ‰ between 1997–2008. We do find that the global value depends strongly on the amount of C_4 photosynthesis prescribed in the model. In addition, we find that with the addition of fire disturbances SiBCASA resolves generally smaller values for the disequilibrium flux than without. It shows the importance of including biomass burning in such a model as it shortens the effective turnover times of the biogeochemical pools. This is especially important for multi-tracer (CO_2 and $^{13}CO_2$) inversion techniques to estimate surface carbon fluxes. More realistic isotopic flux estimates will eventually lead to a better estimated land/ocean mean flux partitioning.

There are some notable differences between our disequilibrium flux and the LPJ simulations presented by Scholze et al. (2008). First of all, their disequilibrium flux in the ISOVAR-NF simulation was much larger compared to their ISOVAR simulation (~ 25 %). This is because their estimates of biomass burning are 4 times larger than ours, which explains the large impact on the disequilibrium flux in their study. They do acknowledge that their global mean value of biomass burning (8 $Pg\,C\,yr^{-1}$) is much larger compared to other studies (e.g. Andreae, 1991). Secondly, their ISOFIX simulation was much less variable compared to their ISOVAR simulation, whereas we still have rather large variabilty in ISOFIX because changes in C_3 and C_4 productivity are a much more important driver of variability in our disequilibrium flux. This is mainly due to the much larger fraction of GPP that is assigned to C_4 productivity. The differences in the mean ISOVAR disequilibrium isofluxes between Scholze et al. (34.8 $Pg\,C\,‰\,yr^{-1}$) and this study (25.8 $Pg\,C\,‰\,yr^{-1}$) at the end of the simulation period is a consequence of differences in the resolved heterotrophic respiration fluxes between the two studies: 69.4 $Pg\,C\,yr^{-1}$ compared to 52.3 $Pg\,C\,yr^{-1}$ in our study.

BGD
11, 107–149, 2014

CC BY

Differences between observed and simulated respiration signatures presented in Figs. 7 and 8 could result from the constants used to estimate C_3 discrimination. Under certain circumstances these parameters are not representative anymore for a specific biome or plant functional type. Experiments have shown that discrimination that is associated with carbon fixation in the chloroplasts could range between 26 ‰ to 38 ‰ depending on plant types and conditions (O'Leary, 1981). As shown in the Methodology section, an in-between value of 28.2 ‰ discrimination is chosen in the discrimination model, which includes the consideration that 5 % of all carbon fixated by C_3 plants is only slightly discriminated because it occurs through reactions with PEPC (Brugnoli and Farquhar, 2000). This fraction that is fixated through PEPC could be different in reality, depending on the type of vegetation. A range from 5 % to 10 % has been reported in the literature (e.g. Lloyd and Farquhar, 1994). Another possibility is that we miss important natural variations in our model, specifically in relative humidity and soil moisture stress.

(3) Atmospheric humidity seems to be an important contributor to the stomatal induced variations in isotopic discrimination and these findings are in agreement with various measurement campaigns. Unfortunately, a strong correlation between the isotopic signature in respiration and humidity as shown in the observations is currently not present in our model. The main reasons are: (1) a generally weak response in discrimination to changes in VPD, (2) the latency in recently assimilated carbon to become available for respiration, and (3) possibly, the absence of additional processes that contribute to additional stomatal stress. An example of an additional process could be anaerobic stress effects. Ometto et al. (2002) speculate that reduced isotope discrimination can also occur when plants are exposed to excess in rainfall. Such a non-linear response in discrimination, (i.e., low discrimination under low precipitation amounts, higher discrimination during moderate precipitation amounts, and again low discrimination during very high precipitation amounts), is not found either in SiBCASA or in SiB2.5 (Suits et al., 2005).

BGD
11, 107–149, 2014

Other discrimination effects after photosynthesis are not considered in SiBCASA when carbon is allocated to the different carbon pools or when carbon is released back to the atmosphere as respiration. These additional fractionation processes produce additional changes and variations in carbon isotope signatures (Brüggemann et al., 2011), but are often very complex to model and are still not fully understood.

This study shows that the isotopic composition of plants can change under influence of environmental conditions and complex discrimination processes. However, measurements suggest that responses to climate anomalies will likely invoke much more variability in the assimilation and respiration signatures than what we currently model, but indirectly it can also invoke more variability in the isotopic disequilibrium. This is important because the disequilibrium flux plays a critical role in closing the atmospheric ^{13}C budget and variability. From a top-down perspective, under the assumption of low ocean variability, the disequilibrium flux must hold a large amount of variability to close the budget with measurements of ^{13}C in CO_2 (Alden et al., 2010). However, from a bottom-up point of view, SiBCASA's disequilibrium flux holds too little variability, which leaves us with a gap in the ^{13}C variability budget (van der Velde et al., 2013). An increase in the sensitivity of stomatal conductance and discrimination, and a better representation of environmental stress towards respiration will play a key role for future improvements in SiBCASA.

The current work identifies a need to better represent the starch dynamics in models to capture changes in environmental stress in respiration signature. Currently the effective turnover of starch is 70 days, which results from the assumption that only 10 % of the storage pool is available for growth. This is assumption is unfortunately less appropriate for representing the exchange of carbon isotopes because most of the day-to-day variations of the carbon isotopic signatures are averaged out in the 2.5 month turnover window of the storage pool. Simply reducing the effective storage pool turnover is not appropriate. It may improve the ^{13}C exchange, but will also alter biomass and fluxes throughout the model, sometimes adversely.

BGD
11, 107–149, 2014

Most models have a single starch pool (if they have one at all), however, these results indicate having two starch pools (fast and slow) is more realistic. The fast starch pool would represent sucrose with a turnover of 7 days and the slow starch pool would represent other carbohydrates and have a turnover of several months. Assimilated carbon would go into the fast pool, which would supply starch for leaf, wood, and root growth. The slow pool would take starch from the fast pool in times of plenty and give starch in lean times. Observations have indicated that the ratios of these two storage pools should be 1 : 10, i.e., 10 % of the carbon in storage is available for growth. The fast starch pool, and thus the isotopic composition of autotrophic respiration that originates from it, would be very responsive to VPD while the slow starch pool would maintain the right amount of total starch to remain consistent with observations. Our future efforts will focus on these improvements together with improvements of SiBCASA's drought response.

Appendix A

Isotopic notation

Isotopes in a given sample are usually expressed as ratio R: a rare compound to an abundant compound. In case of ^{13}C,

$$R = \frac{\text{rare}}{\text{abundant}} = \frac{^{13}C}{^{12}C}. \tag{A1}$$

In nature, differences in ratios between samples are often very small. Therefore, sampled isotopic ratios are compared to a common standard ratio, which is measured in carbonate rock Pee Dee Belemnite (PDB). Deviations from the standard are expressed

BGD
11, 107–149, 2014

in per mille (‰), and are defined as

$$\delta^{13}C_{sample} = \left(\frac{\left[{}^{13}C/{}^{12}C\right]}{\left[{}^{13}C/{}^{12}C\right]_{std}} - 1 \right) \times 1000 \tag{A2}$$

$$= \left(\frac{R_{sample}}{R_{std}} - 1 \right) \times 1000, \tag{A3}$$

where $R_{std} = 0.0112372$ (PDB standard, Craig, 1957). That means that roughly 1.1 % of the carbon exists in the form of ${}^{13}C$. Negative values of $\delta^{13}C$ indicate that the isotopic ratio R_{sample} is smaller than the PDB standard, i.e., the sample is more depleted in ${}^{13}C$. If $\delta^{13}C$ is positive the sample is more enriched in ${}^{13}C$.

During certain processes, like e.g. photosynthesis, isotopic ratios can change under influence of molecular diffusion or chemical reactions. For instance, the isotopic ratio in recent assimilated carbon in a plant is smaller than the isotopic ratio of carbon in atmospheric CO_2 ($R_{ab} < R_{atm}$). This effect is also called isotopic discrimination and it can be expressed as the ratio of R_{atm}/R_{ab}. Discrimination is often expressed in ‰, just like for the isotopic signatures in samples, i.e.,

$$\Delta = \left(\frac{R_{atm}}{R_{ab}} - 1 \right) \times 1000 \approx \delta^{13}C_{atm} - \delta^{13}C_{ab}, \tag{A4}$$

and is often a desirable notation because strength of discrimination between samples can be approximated by the difference in isotopic signatures. If $R_{atm}/R_{ab} = 1$, which means that the isotopic signatures in both samples are the same, would give $\Delta = 0$ ‰ (no discrimination). On the other hand, if $R_{atm}/R_{ab} > 1$, we would compute $\Delta > 0$ ‰.

Acknowledgements. We thank all the people involved in the BASIN measurement campaigns and Louis Giglio for sharing the GFED version 3 burned area data. This project was funded and supported by a VIDI grant (5120490-01) and a grant for computing time (SH-060-13) from the Netherlands Organization for Scientific Research (NWO).

References

Alden, C. B., Miller, J. B., and White, J. W. C.: Can bottom-up ocean CO_2 fluxes be reconciled with atmospheric ^{13}C observations?, Tellus B, 62, 369–388, doi:10.1111/j.1600-0889.2010.00481.x, 2010. 109, 110, 117, 130

Andreae, M. O.: Biomass burning: its history, use, and distribution and its impact on environmental quality and global change, in: Global Biomass Burning: Atmospheric, Climatic, and Biospheric Implications, edited by: Levine, J. S., MIT Press, Cambridge, USA, 3–21, 1991. 128

Ballantyne, A. P., Miller, J. B., and Tans, P. P.: Apparent seasonal cycle in isotopic discrimination of carbon in the atmosphere and biosphere due to vapor pressure deficit, Global Biogeochem. Cy., 24, GB3018, doi:10.1029/2009GB003623, 2010.

Bowling, D. R., McDowell, N. G., Bond, B. J., Law, B. E., and Ehleringer, J. R.: ^{13}C content of ecosystem respiration is linked to precipitation and vapor pressure deficit, Oecologia, 131, 113–124, 2002. 125, 126, 149

Brugnoli, E. and Farquhar, G. D.: Photosynthetic fractionation of carbon isotopes, in: Photosynthesis: Physiology and Metabolism, edited by: Leegood, R. C., Sharkey, T. D., and von Caemmerer, S., Kluwer Acad., Norwell, Mass., 399–434, 2000. 129

Brüggemann, N., Gessler, A., Kayler, Z., Keel, S. G., Badeck, F., Barthel, M., Boeckx, P., Buchmann, N., Brugnoli, E., Esperschütz, J., Gavrichkova, O., Ghashghaie, J., Gomez-Casanovas, N., Keitel, C., Knohl, A., Kuptz, D., Palacio, S., Salmon, Y., Uchida, Y., and Bahn, M.: Carbon allocation and carbon isotope fluxes in the plant-soil-atmosphere continuum: a review, Biogeosciences, 8, 3457–3489, doi:10.5194/bg-8-3457-2011, 2011. 115, 130

Ciais, P., Tans, P. P., White, J., and Trolier, M.: Partitioning of ocean and land uptake of CO_2 as inferred by $\delta^{13}C$ measurements from the NOAA climate monitoring and diagnostics laboratory global air sampling network, J. Geophys. Res., 100, 5051–5070, 1995. 109

Collatz, G. J., Ball, J., Grivet, C., and Berry, J. A.: Physiological and environmental regulation of stomatal conductance, photosynthesis and transpiration: a model that includes a laminar boundary layer, Agr. Forest Meteorol., 54, 107–136, 1991. 112

Collatz, G. J., Ribas-Carbo, M., and Berry, J. A.: Coupled photosynthesis-stomatal conductance model for leaves of C4 plants, Aust. J. Plant Physiol., 19, 519–538, 1992. 112

BGD
11, 107–149, 2014

Craig, H.: The geochemistry of stable carbon isotopes, Geochim. Cosmochim. Ac., 3, 53–92, 1953. 114

Craig, H.: Isotopic standards for carbon and oxygen and correction factors for mass-spectrometric analysis of carbon dioxide, Geochim. Cosmochim. Ac., 12, 133–149, 1957. 132

Ehleringer, J. R. and Cook, C. S.: Carbon and oxygen isotope ratios of ecosystem respiration along an Oregon conifer transect: preliminary observations based upon small-flask sampling, Tree Physiol., 18, 513–519, 1998. 125

Ekblad, A. and Hogberg, P.: Natural abundance of ^{13}C in CO_2 respired from forest soils reveals speed of link between tree photosynthesis and root respiration, Oecologia, 127, 305–308, 2001. 125, 126, 149

Farquhar, G. D.: On the nature of carbon isotope discrimination in C_4 species, Aust. J. Plant Physiol., 10, 205–226, 1983. 114

Farquhar, G. D., Caemmerer, S. V., and Berry, J. A.: A biochemical-model of photosynthetic CO_2 assimilation in leaves of C_3 species, Planta, 149, 78–90, 1980. 112

Farquhar, G. D., Ehleringer, J. R., and Hubrick, K. T.: Carbon isotope discrimination and photosynthesis, Annu. Rev. Plant Phys., 40, 503–537, 1989. 109

Francey, R. J., Tans, P. P., Allison, C. E., Enting, I. G., White, J. W. C., and Trolier, M.: Changes in oceanic and terrestrial carbon uptake since 1982, Nature, 373, 326–330, 1995. 123

Francey, R. J., Allison, C. E., Etheridge, D. M., Trudinger, C. M., Enting, I. G., Leuenberger, M., Langenfelds, R. L., Michel, E., and Steele, L. P.: A 1000-year high precision record of delta C-13 in atmospheric CO_2, Tellus B, 51, 170–193, 1999. 117, 119

Fung, I., Field, C. B., Berry, J. A., Thompson, M. V., Randerson, J. T., Malmström, C. M., Vitousek, P. M., James Collatz, G., Sellers, P. J., Randall, D. A., Denning, A. S., Badeck, F., and John, J.: Carbon 13 exchanges between the atmosphere and biosphere, Global Biogeochem. Cy., 11, 507–533, 1997. 110, 122

Giglio, L., Randerson, J. T., van der Werf, G. R., Kasibhatla, P. S., Collatz, G. J., Morton, D. C., and DeFries, R. S.: Assessing variability and long-term trends in burned area by merging multiple satellite fire products, Biogeosciences, 7, 1171–1186, doi:10.5194/bg-7-1171-2010, 2010. 118

Gurney, K. R., Law, R. M., Denning, A. S., Rayner, P. J., Baker, D., Bousquet, P., Bruhwiler, L., Chen, Y. H., Ciais, P., Fan, S., Fung, I. Y., Gloor, M., Heimann, M., Higuchi, K., John, J., Maki, T., Maksyutov, S., Masarie, K., Peylin, P., Prather, M., Pak, B. C., Randerson, J., Sarmiento,

J., Taguchi, S., Takahashi, T., and Yuen, C. W.: Towards robust regional estimates of CO_2 sources and sinks using atmospheric transport models, Nature, 415, 626–630, 2002. 110, 120

Indermuhle, A., Stocker, T. F., Joos, F., Fischer, H., Smith, H. J., Wahlen, M., Deck, B., Mastroianni, D., Tschumi, J., Blunier T., Meyer, R., and Stauffer, B. : Holocene carbon-cycle dynamics based on CO_2 trapped in ice at Taylor Dome, Antarctica, Nature, 398, 121–126, 1999. 119

Joos, F. and Bruno, M.: Long-term variability of the terrestrial and oceanic carbon sinks and the budgets of the carbon isotopes C-13 and C-14, Global Biogeochem. Cy., 12, 277–295, 1998. 123

Kaplan, J. O., Prentice, I. C., and Buchmann, N.: The stable carbon isotope composition of the terrestrial biosphere: modeling at scales from the leaf to the globe, Global Biogeochem. Cy., 16, 1060, doi:10.1029/2001GB001403, 2002. 110, 122

Keeling, C. D.: The Suess effect: 13Carbon–14Carbon interrelations, Environ. Int., 2, 229–300, 1979. 110

Keeling, C. D. and Revelle, R.: Effects of El Nino/Southern Oscillation on the atmospheric content of carbon dioxide, Meteoritics, 20, 437–450, 1985. 109

Keeling, C. D., Bacastow, R. B., Carter, A. F., Piper, S. C., Whorf, T. P., Heimann, M., Mook, W. G., and Roeloffzen, H.: A three-dimensional model of atmospheric CO_2 transport based on observed winds: 1. Analysis of observational data, in: Aspects of Climate Variability in the Pacific and the Western Americas, edited by: Peterson, D. H., American Geophysical Union, Washington D.C., USA, 165–236, 1989. 109

Lloyd, J. and Farquhar, G. D.: ^{13}C discrimination during CO_2 assimilation by the terrestrial biosphere, Oecolgia, 99, 201–215, 1994. 110, 122, 129

Masarie, K. A. and Tans, P. P.: Extension and integration of atmospheric carbon-dioxide data into a globally consistent measurement record, J. Geophys. Res.-Atmos., 100, 11593–11610, 1995. 119

Mook, W. G., Bommerson, J. G., and Staverman, W. H.: Carbon isotope fractionation between dissolved bicarbonate and gaseous carbon dioxide, Earth Planet. Sc. Lett., 22, 169–176, 1974. 114

Nakazawa, T., Morimoto, S., Aoki, S., and Tanaka, M.: Time and space variations of the carbon isotopic ratio of tropospheric carbon dioxide over Japan, Tellus B, 45, 258–274, 1993. 109

O'Leary, M. H.: Carbon isotope fractionation in plants, Phytochemistry, 20, 553–567, 1981. 129

O'Leary, M. H.: Measurement of the isotopic fractionation associated with diffusion of carbon dioxide in aqueous solution, J. Phys. Chem., 88, 823–825, 1984. 114

Ometto, J. P. H. B., Flanagan, L. B., Martinelli, L. A., Moreira, M. Z., Higuchi, N., and Ehleringer, J. R.: Carbon isotope discrimination in forest and pasture ecosystems of the Amazon Basin, Brazil, Global Biogeochem. Cy., 16, 1109, doi:10.1029/2001GB001462, 2002. 125, 129

Page, S. E., Siegert, F., Rieley, J. O., Boehm, H. D. V., Jaya, A., and Limin, S.: The amount of carbon released from peat and forest fires in Indonesia during 1997, Nature, 420, 61–65, doi:10.1038/nature01131, 2002. 119

Pataki, D. E., Ehleringer, J. R., Flanagan, L. B., Yakir, D., Bowling, D. R., Still, C. J., Buchmann, N., Kaplan, J. O., and Berry, J. A.: The application and interpretation of Keeling plots in terrestrial carbon-cycle research, Global Biogeochem. Cy., 17, 1022, doi:10.1029/2001GB001850, 2003. 124, 148

Peters, W., Jacobson, A. J., Sweeney, C., Andrews, A. E., Conway, T. J., Masarie, K., Miller, J. B., Bruhwiler, L. M. P., Petron, G., Hirsch, A. I., Worthy, D. E. J., Van der Werf, G. R., Randerson, J. T., Wennberg, P. O., Krol, M. C., and Tans, P. P.: An atmospheric perspective on North American carbon dioxide exchange: CarbonTracker, P. Natl. Acad. Sci. USA, 107, 18925–18930, 2007. 110

Peters, G. P., Marland, G., Quere, C. L., Boden, T., Canadell, J. G., and Raupach, M. R.: Rapid growth in CO_2 emissions after the 2008–2009 global financial crisis, Nat. Clim. Change, 2, 2–4, 2012. 109

Potter, C. S., Randerson, J. T., Field, C. B., Matson, P. A., Vitousek, P. M., Mooney, H. A., and Klooster, S. A.: A process-oriented model based on global satellite and surface data, Global Biogeochem. Cy., 7, 811–842, 1995. 112

Ramankutty, N. and Foley, J. A.: Characterizing patterns of global land use: an analysis of global croplands data, Global Biogeochem. Cy., 12, 667–686, 1998. 122

Randerson, J. T., Thompson, M. V., Malmstrom, C. M., Field, C. B., and Fung, I. Y.: Substrate limitations for heterotrophs: implications for models that estimate the seasonal cycle of atmospheric CO_2, Global Biogeochem. Cy., 10, 585–602, 1996.

Rayner, P. J., Law, R. M., Allison, C. E., Francey, R. J., Trudinger, C. M., and Pickett-Heaps, C.: Interannual variability of the global carbon cycle (1992–2005) inferred by inversion of atmospheric CO_2 and $\delta^{13}CO_2$ measurements, Global Biogeochem. Cy., 22, GB3008, doi:10.1029/2007GB003068, 2008. 109

Schaefer, K., Collatz, G. J., Tans, P. P., Denning, A. S., Baker, I., Berry, J. A., Prihodko, L., Suits, N., and Philpott, A.: Combined Simple Biosphere/Carnegie-Ames-Stanford Approach terrestrial carbon cycle model, J. Geophys. Res., 113, G03034, doi:10.1029/2007JG000603, 2008. 111, 112, 113, 119

Scholze, M., Kaplan, J. O., Knorr, W., and Heimann, M.: Climate and interannual variability of the atmosphere-biosphere $^{13}CO_2$ flux, Geophys. Res. Lett., 30, 1097, doi:10.1029/2002GL015631, 2003. 110, 119, 122

Scholze, M., Ciais, P., and Heimann, M.: Modeling terrestrial ^{13}C cycling: climate, land use and fire, Global Biogeochem. Cy., 22, GB1009, doi:10.1029/2006GB002899, 2008. 110, 115, 123, 128

Sellers, P. J., Tucker, C. J., Collatz, G. J., Los, S. O., Justice, C. O., Dazlich, D. A., and Randall, D. A.: A global 1 by 1 NDVI data set for climate studies – Part 2: The generation of global fields of terrestrial biosphysical parameters from NDVI, Int. J. Remote. Sens., 15, 3519–3545, 1994. 112

Sellers, P. J., Randall, D. A., Collatz, G. J., Berry, J. A., Field, C. B., Dazlich, D. A., Zhang, C., Collelo, G. D., and Bounoua, L.: A revised land surface parameterization (SiB2) for atmospheric GCMs – Part 1: Model formulation, J. Climate, 9, 676–705, 1996a. 112

Sellers, P. J., Los, S. O., Tucker, C. J., Justice, C. O., Dazlich, D. A., Collatz, G. J. and Randall, D. A.: A revised land surface parameterization (SiB2) for atmospheric GCMs – Part 2: The generation of global fields of terrestrial biophysical parameters from satellite data, J. Climate, 9, 706–737, 1996b.

Siegenthaler, U. and Oeschger, H.: Biospheric CO_2 emissions during the past 200 years reconstructed by deconvolution of ice core data, Tellus B, 39, 140–154, 1987. 109

Still, C. J., Berry, J. A., Collatz, G. J., and DeFries, R. S.: Global distribution of C-3 and C-4 vegetation: carbon cycle implications, Nature Climate Change, 17, 1006–1019, 2003. 109, 112, 122, 125

Suess, H. E.: Radiocarbon concentration in modern wood, Science, 122, 415–417, 1955. 110

Suits, N., Denning, A., Berry, J., and Still, C.: Simulation of carbon isotope discrimination of the terrestrial biosphere, Global Biogeochem. Cy., 19, GB1017, doi:10.1029/2003GB002141, 2005. 110, 111, 113, 114, 115, 122, 125, 129

Tans, P. P.: On calculating the transfer of C-13 in reservoir models of the carbon-cycle, Tellus, 32, 464–469, 1980.

BGD
11, 107–149, 2014

CC BY

Tans, P. P., Berry, J. A., and Keeling, R. F.: Oceanic $^{13}C/^{13}C$ observations – a new window on ocean CO_2 uptake, Global Biogeochem. Cy., 7, 353–368, 1993. 109

van der Velde, I. R., Miller, J. B., Schaefer, K., Masarie, K. A., Denning, S., White, J. W. C., Tans, P. P., Krol, M. C., and Peters, W.: Biosphere model simulations of interannual variability in terrestrial 13C/12C exchange, Global Biogeochem. Cy., 27, 637–649, 2013. 110, 111, 117, 119, 122, 130

van der Werf, G. R., Randerson, J. T., Collatz, G. J., and Giglio, L.: Carbon emissions from fires in tropical and subtropical ecosystems, Glob. Change Biol., 9, 547–562, 2003.

van der Werf, G. R., Randerson, J. T., Giglio, L., Collatz, G. J., Kasibhatla, P. S., and Arellano Jr., A. F.: Interannual variability in global biomass burning emissions from 1997 to 2004, Atmos. Chem. Phys., 6, 3423–3441, doi:10.5194/acp-6-3423-2006, 2006. 120

van der Werf, G. R., Dempewolf, J., Trigg, S. N., Randerson, J. T., Kasibhatla, P. S., Giglio, L., Murdiyarso, D., Peters, W., Morton, D. C., Collatz, G. J., Dolman, A. J., and DeFries, R. S.: Climate regulation of fire emissions and deforestation in equatorial Asia, P. Natl. Acad. Sci. USA, 105, 20350–20355, 2008. 111

van der Werf, G. R., Randerson, J. T., Giglio, L., Collatz, G. J., Mu, M., Kasibhatla, P. S., Morton, D. C., DeFries, R. S., Jin, Y., and van Leeuwen, T. T.: Global fire emissions and the contribution of deforestation, savanna, forest, agricultural, and peat fires (1997–2009), Atmos. Chem. Phys., 10, 11707–11735, doi:10.5194/acp-10-11707-2010, 2010. 111, 117, 120, 121, 127

Vidale, P. L. and Stockli, R.: Prognostic canopy air space solutions for land surface exchanges, Theor. Appl. Climatol., 80, 245–257, 2005. 112

Wingate, L., Ogee, J., Burlett, R., Bosc, A., Devaux, M., Grace, J., Loustau, D., and Gessler, A.: Photosynthetic carbon isotope discrimination and its relationship to the carbon isotope signals of stem, soil and ecosystem respiration, New Phytol., 188, 576–589, 2010. 109

BGD
11, 107–149, 2014

Table 1. Combustion completeness fractions for different biomes and carbon pools. The tree mortality fraction is given in the last column. Both quantities are chosen accordingly to represent the biome mean value. CWD stands for coarse woody debris, and surfmet, surfstr, and surfmic stand respectively for surface metabolic, surface structural, and surface microbial.

biomes	storage	leaf	wood	CWD	surfmet	surfstr	surfmic	mortality
tropical forests	0.9	0.9	0.5	0.2	0.9	0.9	0.9	0.9
deciduous forests	0.8	0.8	0.2	0.4	0.8	0.8	0.8	0.6
mixed deciduous forests	0.8	0.8	0.2	0.4	0.8	0.8	0.8	0.6
taiga forest, boreal forest	0.8	0.8	0.2	0.4	0.8	0.8	0.8	0.6
mixed taiga forest, boreal forest	0.8	0.8	0.2	0.4	0.8	0.8	0.8	0.6
mixed trees and grasslands	0.9	0.9	0.3	0.5	0.9	0.9	0.9	0.05
pure grasslands	0.9	0.9	0.3	0.9	0.9	0.9	0.9	0.01
dry grasslands	0.9	0.9	0.3	0.9	0.9	0.9	0.9	0.01
tundra	0.8	0.8	0.2	0.4	0.8	0.8	0.8	0.6
desert	0.9	0.9	0.3	0.9	0.9	0.9	0.9	0.01
agriculture	0.9	0.9	0.3	0.9	0.9	0.9	0.9	0.01

BGD
11, 107–149, 2014

Table 2. Description of the three different simulations. (+) means process is included in the simulation and (–) means the process is not included.

name simulation	variable C_3 fractionation	variable δ_a	fire	run time
ISOVAR	+	+	+	1851–2010
ISOFIX	– (kept constant at 19.2)	+	+	1851–2010
ISOVAR-NF	+	+	–	1851–2010

BGD
11, 107–149, 2014

Table 3. Comparison of isotopic parameters between different modeling studies.

	% C_4 GPP	C_3 Δ [‰]	C_4 Δ [‰]	net Δ [‰]	Isodis. coeff. (1987/1988) [‰]	D_{bio} (1987/1988) [PgC‰yr^{-1}]
Lloyd and Farquhar (1994)	21	17.8	3.6	14.8	n/a	n/a
Francey et al. (1995)	n/a	n/a	n/a	18.0	0.43	25.8
Fung et al. (1997)	27	20.0	4.4	15.7	0.33	n/a
Joos and Bruno (1998)	n/a	n/a	n/a	18.7	0.43	26.4
Kaplan et al. (2002)	15	20.0	3 to 4	18.1	n/a	n/a
Scholze et al. (2003, 2008)	less than 10	10 to 23	3 to 4	17.7	0.42–0.59	23.8–41.8
Suits et al. (2005)	24	19.2	4.4	15.9	n/a	n/a
SiBCASA (this study)	30	19–20	4.4	15.2	0.42	21.2

BGD
11, 107–149, 2014

CC BY

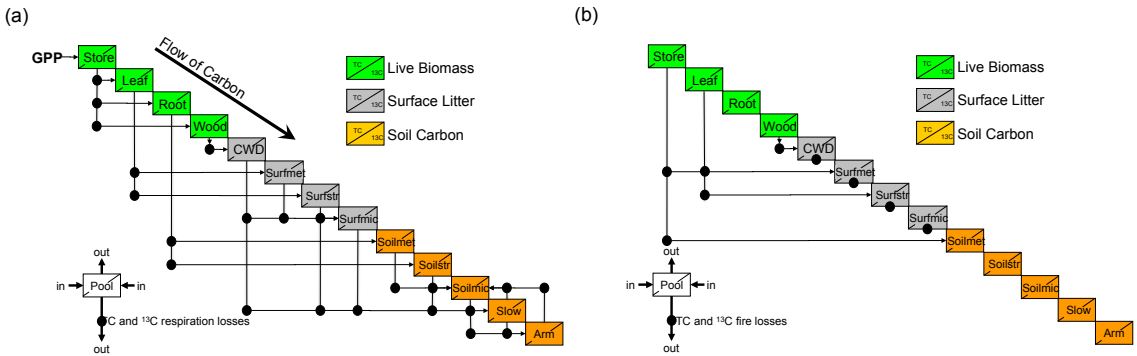

Fig. 1. The modified SiBCASA pool configuration **(a)**, where each box represents a total carbon (TC) and a ^{13}C pool. Carbon generally flows from upper left to lower right: vertical lines are losses from each pool, horizontal arrows are gains to each pool, and dots represent the transfer of carbon from one pool to another, where a fraction is lost to the atmosphere as respiration. GPP minus the canopy respiration puts starch into the storage pool, which becomes available for growth and maintenance of leafs, roots, and wood. Dying of biomass is mimicked by transferring carbon to the structural, metabolic and microbial surface and soil pools. The autotrophic respiration results from growth and maintenance in the live biomass pools and heterotrophic respiration results from microbial decay in the surface litter and soil carbon pools. The other pool configuration displays specifically the carbon flow introduced by fire disturbances **(b)**. Vertical lines represent pool losses, horizontal lines represent pool gains, and dots represent the TC and ^{13}C fire losses to the atmosphere.

BGD
11, 107–149, 2014

CC BY

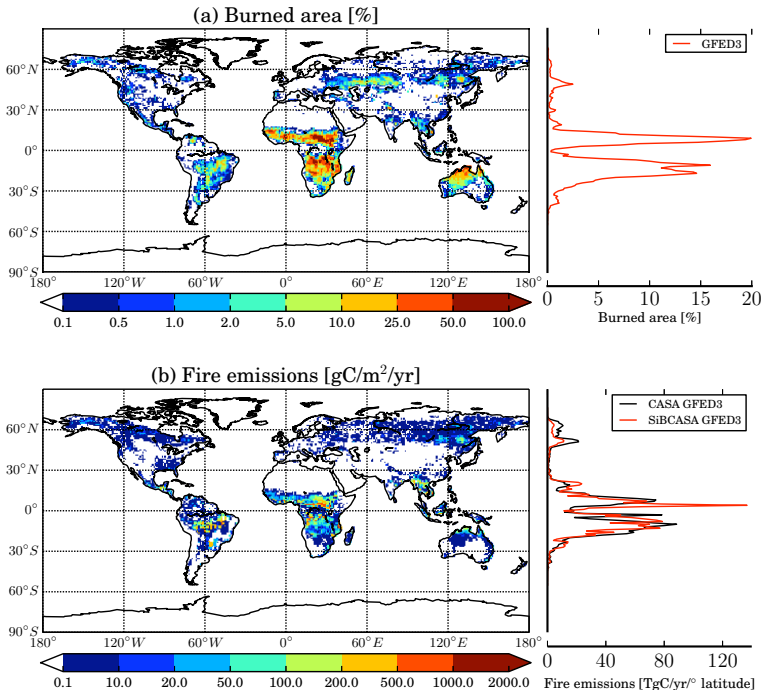

Fig. 2. The **(a)** annual burned area [% per 1° × 1°] from CASA-GFED3 and **(b)** SiBCASA's fire emissions [$gC\,m^{-2}\,yr^{-1}$] averaged over 1997–2009. The color scales in both panels are non-linear. The panels on the right-hand side display the zonal averages of burned area and fire emissions per degree latitude respectively. The fire emissions are the product of burned area and the amount of standing biomass (fuel consumption). Neglecting emissions from organic soils explains the underestimation in the Northern Hemisphere compared to CASA-GFED3 (black line).

BGD
11, 107–149, 2014

CC BY

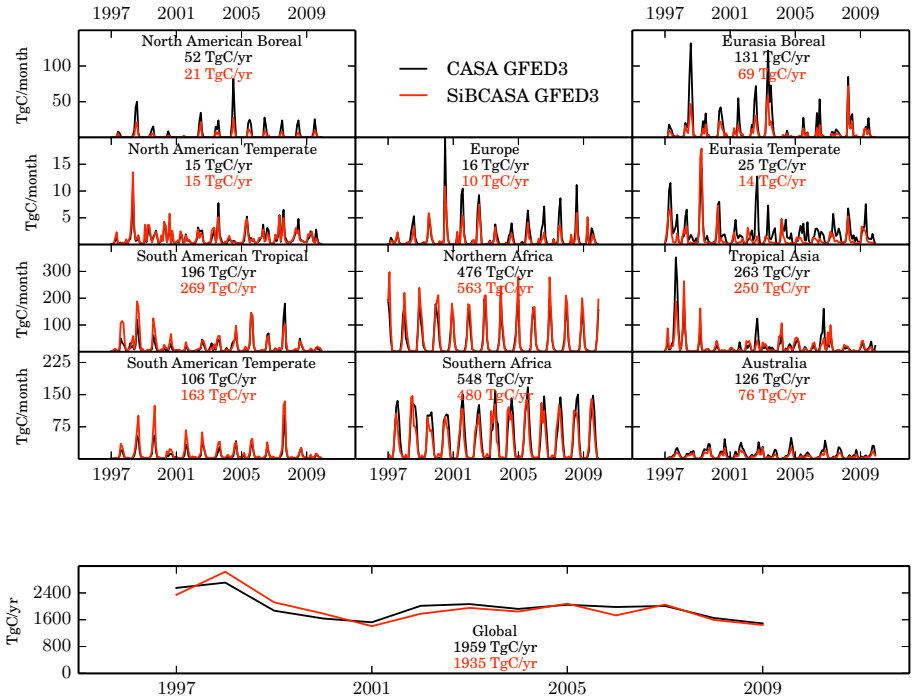

Fig. 3. Monthly fire emissions (TgC month^{-1}) over 1997–2009 for 11 different TransCom regions. CASA-GFED3 (black) is compared to SiBCASA-GFED3 (red) estimates. The multi-year averages for each region are given as values in TgC yr^{-1}. The regions geographically ordered with on the top-left panel North America Boreal and on the lower-right panel Australia. Horizontally, the panels share the same y-axis. The global annual fire emissions (TgC yr^{-1}) for both simulations are displayed in the separate panel below.

BGD
11, 107–149, 2014

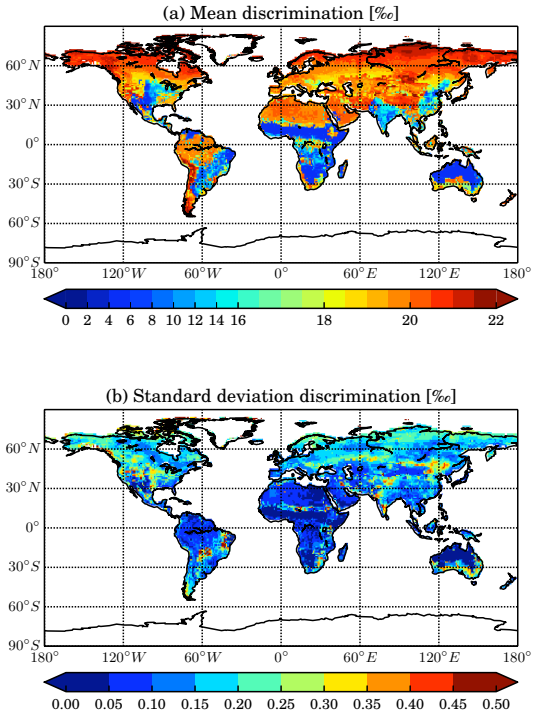

Fig. 4. SiBCASA-ISOVAR assimilation-weighted annual plant discrimination **(a)**, from a 13 yr period (1997–2009), and the year-to-year variability (1σ) of the annual discrimination values determined from the same 13 yr period **(b)**. Differences in C_3 and C_4 metabolic pathways gives the clear spatial contrast in the annual mean discrimination. Variations in gridcell average discrimination are largely driven by RH, precipitation and soil moisture conditions. The largest standard deviations are found in parts of South America and Africa in mixed C_3/C_4 grid cells, where independent changes in C_3 or C_4 GPP can change grid cell mean discrimination value significantly. Note that the color scale in **(a)** is non-linear.

BGD
11, 107–149, 2014

CC BY

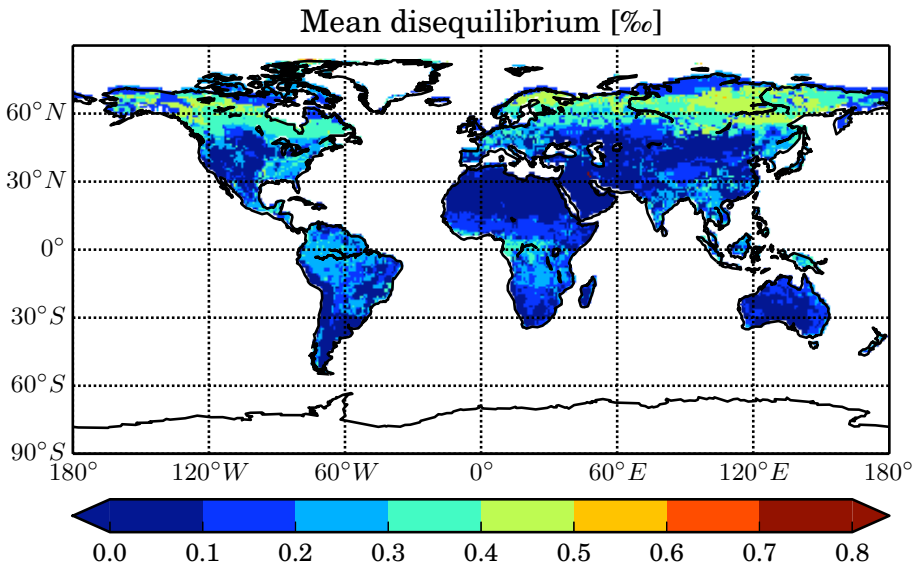

Fig. 5. SiBCASA-ISOVAR disequilibrium coefficient [‰], averaged for a 12 yr period (1997–2008).

BGD
11, 107–149, 2014

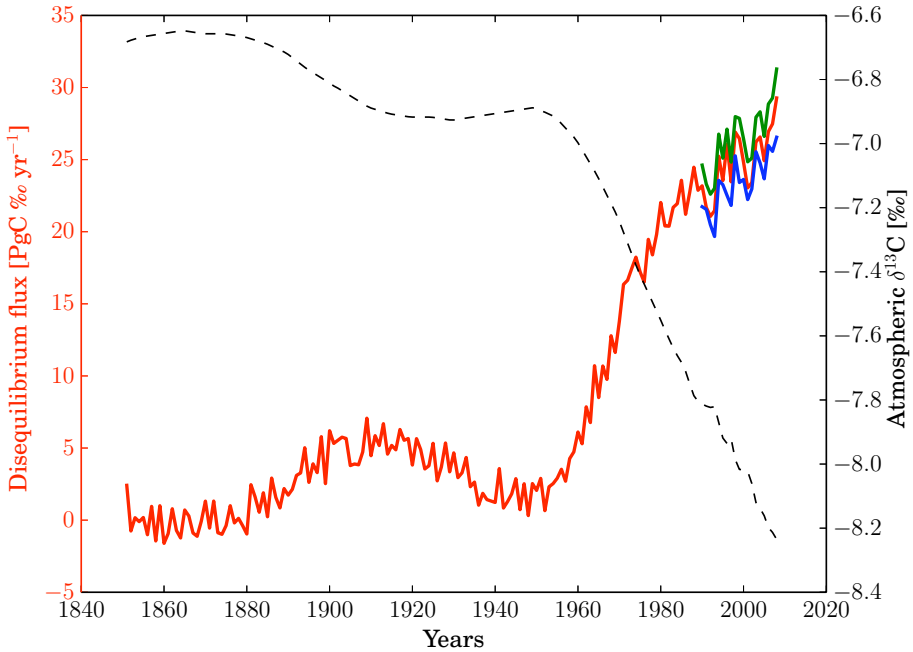

Fig. 6. Time-series (1851–2008) of the global annual disequilibrium flux for three different experiments: ISOVAR (red), ISOFIX (blue) and ISOVAR-NF (green). The ISOFIX and ISOVAR-NF simulations are only shown for the period 1990–2008. Since disequilibrium is strongly linked with atmospheric isotopic composition, δ_a (dashed) is added on the secondary *y* axis.

BGD
11, 107–149, 2014

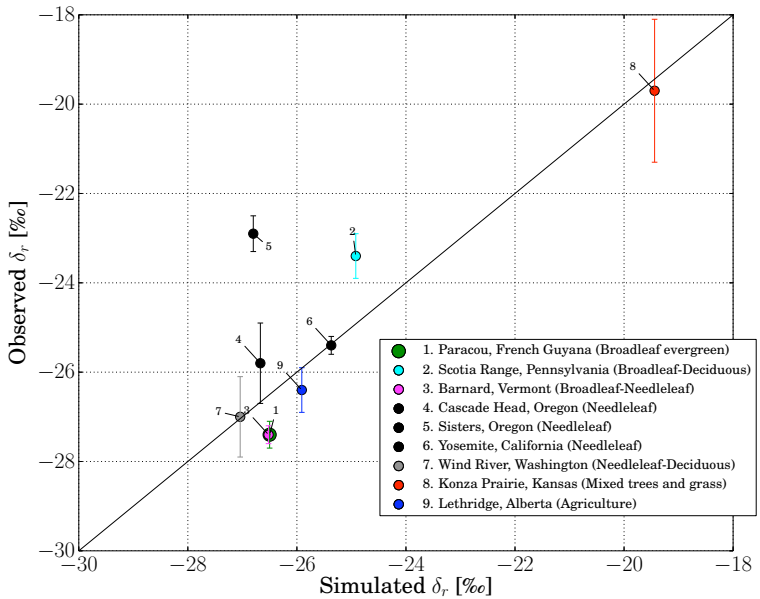

Fig. 7. Measured and modeled signature of respiration at 9 different sites in North and South America. The measurements are from the BASIN network (Pataki et al., 2003), taken in the 1980s and 1990s in the spring and summer months. Each reported value in the figure represents the mean and 1σ standard error over a number of separate measurements which was held at each particular site, and each simulated value was averaged over the same measurement period. The colors indicate the type of biome each site is part of. Overall, our mean simulated respiration signatures compare well with the observations. Outliers seen in this figure might indicate differences between the prescribed carbon turnover and the actual carbon turnover. It could also indicate SiBCASA's inability to capture droughts events that could cause a larger seasonal change in the respiration signature.

BGD
11, 107–149, 2014

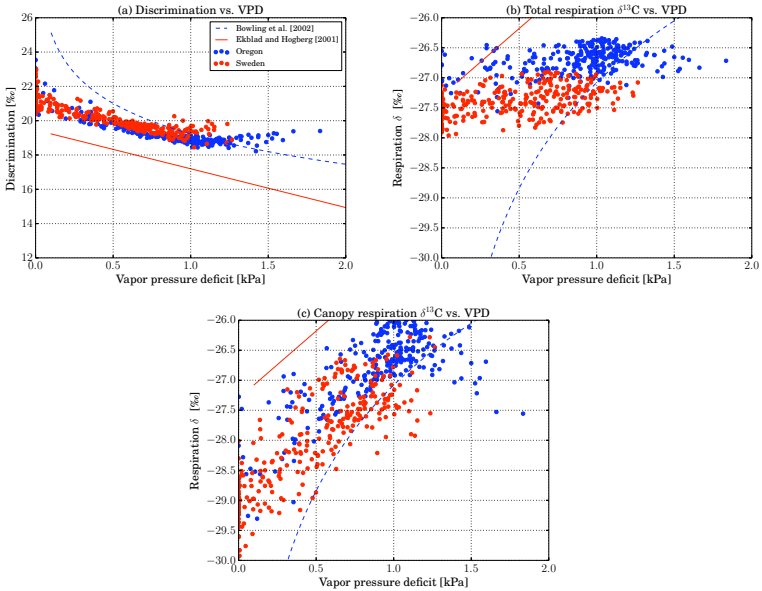

Fig. 8. Plant discrimination [‰] and isotopic signature in respiration [‰] as a function of the vapor pressure deficit (VPD, kPa) for two locations: Oregon (blue) and Sweden (red). In panel **(a)** discrimination vs. VPD. In panel **(b)** the isotopic signatures in total respiration (δ_r) vs. VPD, and in panel **(c)** the isotopic signatures in only canopy respiration vs. VPD. The daily mean values are from the SiBCASA-ISOVAR simulation taken for the summer months in 2000, 2001 and 2002 (May, June, July and August). The daily mean VPD is derived from daylight hours. In the middle and right panel, the dashed line represents a logarithmic fit to measured δ_r taken from sites in Oregon (Bowling et al., 2002). The solid line represents a linear fit to measured δ_r in a mixed coniferous boreal forest in northern Sweden (Ekblad and Hogberg, 2001). In panel **(a)** both lines are approximated as plant discrimination using the relationship: $\Delta = \frac{\delta_a - \delta_r}{\delta_r/1000+1}$.

BGD
11, 107–149, 2014

CC BY